Renormalized ladder-type expansions for many-particle propagators

John M. Herbert*
Theoretical Chemistry Institute and Department of Chemistry, University of Wisconsin, Madison, Wisconsin 53706
(Received 30 April 2002; revised 14 August 2002; published 12 November 2002)

For a system of indistinguishable fermions with pairwise interactions, we consider renormalized, perturbative expansions for the three- and four-particle propagators (Green's functions) in terms of exact one-particle propagators, along with a pair interaction that may be bare (as it appears in the Hamiltonian) or dressed (polarized). Care is taken to provide a rigorous foundation for the diagrammatic representations of these perturbation series; in particular, it is demonstrated how each topologically distinct diagram represents an embedding (in three-dimensional space) of numerous separate terms in the perturbation series. Within a renormalized ladder approximation for the three- and four-particle propagators, we derive diagram weights (which differ from the two-particle diagram weights) in order to limit the perturbation series to topologically distinct, permutationally independent diagrams. These results lay the foundation for perturbative approximations that decouple the propagator and density matrix equations of motion.

DOI: 10.1103/PhysRevA.66.052502 PACS number(s): 31.10.+z, 05.30.Fk, 71.10.−w, 31.15.Md

I. INTRODUCTION

Diagrammatic perturbation theory figures prominently in quantum-theoretical methods based upon the one- or two-particle propagator (Green's function) [1–5]. In principle, a similar diagrammatic formalism exists for the p-particle propagator $\mathbf{G}^{(p)}$, for any p, but propagators for $p>2$ are seldom discussed. The obvious reason is that $\mathbf{G}^{(2)}$—to the extent that one can calculate it—provides most of the important information about a system of N indistinguishable particles, including ground-state expectation values, excitation energies, and quasiparticle energies (ionization potentials and affinities).

Yet there is reason to investigate the propagators $\mathbf{G}^{(3)}$ and $\mathbf{G}^{(4)}$ because these functions are coupled in a nontrivial way to $\mathbf{G}^{(1)}$, $\mathbf{G}^{(2)}$, and the one-particle self-energy by means of certain hierarchies of integro-differential equations of motion [2,6–12]. In an appropriate time-independent limit, $\mathbf{G}^{(p)}$ affords the p-particle reduced density matrix (p-RDM), and the density matrices for different p are also coupled by various hierarchies of equations [13–19]. Of these, the contracted Schrödinger equation [16–26] has recently garnered attention within the quantum chemistry literature. Decoupling of these hierarchies via a suitable application of perturbation theory [16,21,22,26] provides a means for direct calculation of the two-particle propagator or density matrix.

In this paper we consider perturbative expansions of $\mathbf{G}^{(3)}$ and $\mathbf{G}^{(4)}$, for a system of indistinguishable fermions subject to pairwise interactions. We present a rigorous discussion of the diagrammatic representations of these series, calling attention to the fact that each topologically distinct diagram is actually an embedding of numerous separate terms in the perturbation series. This is true (and well known) for the $\mathbf{G}^{(1)}$ and $\mathbf{G}^{(2)}$ perturbation series as well; however, three- and four-particle diagrams exhibit a greater degree of degeneracy and are generally more complicated than one- and two-particle diagrams. One must enumerate the extent of this diagrammatic degeneracy, by means of certain symmetry coefficients, if the perturbation series are to be expressed in terms of topologically distinct diagrams alone.

The present work lays the foundation for perturbative decoupling approximations for the many-particle propagators, leading in the time-independent limit to a decoupling of the contracted Schrödinger equation and thus an equation for the direct determination of the 2-RDM. The author's interest lies in molecular electronic structure, whose physics is dominated by pair correlations between electrons [27], despite the long-range nature of the Coulomb interaction. Under such circumstances, an appropriate starting point for decoupling the propagator or density matrix hierarchies is a ladder approximation for the many-particle propagators, since ladder diagrams (as defined in Sec. IV) account for multiple scattering events between pairs of particles but neglect simultaneous three-particle correlations.

Ladder-type expansions for $\mathbf{G}^{(2)}$ are well known [1] and relatively straightforward, but three- and four-particle ladder diagrams can become rather complicated when both direct and exchange contributions are included. Even within the ladder approximation, diagrams proliferate rapidly as the order in perturbation theory increases, and brute-force enumeration of these diagrams quickly becomes infeasible. In this paper, we systematize the derivation of three- and four-particle ladder diagrams by demonstrating (i) that each ''twisted'' ladder is equivalent to some permutation of a simple, untwisted one; and (ii) that the untwisted ladders can be obtained in a systematic fashion. This is accomplished by means of an algorithm, introduced herein, that generates the precise set of untwisted, topologically distinct three- and four-particle ladder diagrams. By exploiting this systematic construction, we are able to derive the symmetry coefficients that account for the twisted ladder diagrams. At nth order, the appropriate coefficient for both the three- and four-particle ladder diagrams is found to be 2^n, whereas the corresponding symmetry factor for two-particle ladders is only 2^{n-1}.

The remainder of this paper is organized as follows. In Sec. II we briefly introduce the propagators, the dressed in-

*Electronic address: herbert@chem.wisc.edu

teraction, and other ingredients of the perturbation theory. Section III focuses on a rigorous presentation of the diagram technique for many-particle propagators, with special attention paid to the issue of diagrammatic degeneracy. In Secs. IV and V, we derive symmetry coefficients for three- and four-particle ladder diagrams, respectively, via the aforementioned algorithmic construction. These results, which are rather technical in nature, are placed in context within Sec. VI, in which we discuss the application of this methodology to decoupling the propagator and density matrix hierarchies. Section VII constitutes a summary.

II. BASIC CONVENTIONS AND NOTATION

Let Ψ be the ground-state wave function for a system of N indistinguishable fermions with time-independent Hamiltonian $\hat{H}=\hat{H}_0+\hat{V}$. In second quantization

$$\hat{H}_0=\sum_k \varepsilon_k \hat{a}_k^\dagger \hat{a}_k \tag{1}$$

and

$$\hat{V}=\frac{1}{2}\sum_{pqrs} \mathbf{V}_{rs}^{pq} \hat{a}_p^\dagger \hat{a}_q^\dagger \hat{a}_s \hat{a}_r, \tag{2}$$

where the $\hat{a}_k^\dagger$ are the creation operators for some orthonormal spin-orbital basis $\{\phi_k\}$.

Expanded in the basis $\{\phi_k\}$, the p-particle propagator (synonymously, the p-particle Green's function) for the quantum state Ψ is a tensor $\mathbf{G}^{(p)}$ with time-dependent elements

$$[(\mathbf{G}^{(p)})_{k_1,\ldots,k_p}^{j_1,\ldots,j_p}](t_1,\ldots,t_p;t_1',\ldots,t_p') = i^p\langle\Psi|\ \hat{\mathcal{T}}(\hat{a}_{j_1}^\dagger(t_1)\cdots\hat{a}_{j_p}^\dagger(t_p)\ \hat{a}_{k_p}(t_p')\cdots\hat{a}_{k_1}(t_1'))|\Psi\rangle. \tag{3}$$

Here $\hat{a}_k(t)\equiv e^{it\hat{H}}\hat{a}_k e^{-it\hat{H}}$ is the Heisenberg representation of $\hat{a}_k$. The operator $\hat{\mathcal{T}}$ is a signed permutation that brings the time-dependent operator product into descending time order from left to right, with creation operators $\hat{a}_k^\dagger$ on the left in the case of equal times. For example,

$$\hat{\mathcal{T}}(\hat{a}_j(t)\ \hat{a}_k^\dagger(t'))=\begin{cases}\hat{a}_j(t)\ \hat{a}_k^\dagger(t') & \text{if } t>t'\\ -\hat{a}_k^\dagger(t')\ \hat{a}_j(t) & \text{if } t\leq t'.\end{cases} \tag{4}$$

A perturbative expansion of $\mathbf{G}^{(p)}$ is obtained in the usual way [1,3]. Nominally, the terms in this series are expectation values of time-ordered operator products, with respect to some single-determinant reference state Ψ_0. Decomposition of these expectation values using Wick's theorem [1] affords an expansion in terms of the one-particle propagator for the reference state Ψ_0. Since our ultimate interest lies in the many-particle propagators, from which one can easily obtain $\mathbf{G}^{(1)}$, it is logical to express all diagrams using exact one-particle propagators. These we represent in diagram form as

$i\left[(\mathbf{G}^{(1)})_k^j\right](t;t') \equiv$ 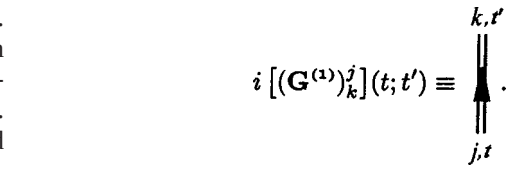 . (5)

A term in the expansion of $\mathbf{G}^{(p)}$ thus consists of p directed $\mathbf{G}^{(1)}$ lines (quasiparticle lines) connected by certain pairwise interactions. In its most primitive form the pair interaction is simply the "bare" interaction $\hat{V}(t)$, expressed in the interaction representation (with respect to $\hat{H}_0$) and represented diagrammatically as

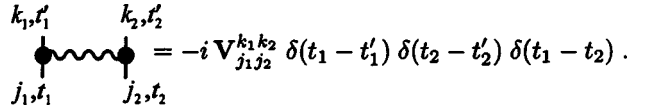 $= -i\,\mathbf{V}_{j_1 j_2}^{k_1 k_2}\,\delta(t_1-t_1')\,\delta(t_2-t_2')\,\delta(t_1-t_2)$. (6)

The δ functions codify the fact that $\hat{V}$ is instantaneous.

The formalism developed herein is equally applicable to a renormalized (synonymously, "polarized" or "dressed") interaction, and we shall represent the pair interaction using a double wiggle to indicate this fact. At present we need not specify the extent of this renormalization, but an illustrative example is the random phase approximation [1,3], in which the effective interaction is given by the sum of pair bubbles

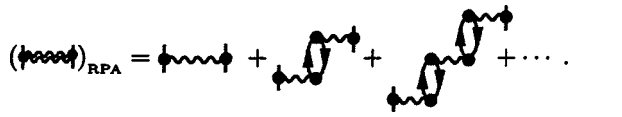 (7)

An important point to note is that virtual particle-hole pairs created and subsequently annihilated by the dressed interaction [as in the latter two diagrams on the right side of Eq. (7)] must propagate through some time interval t_2-t_1, hence the dressed interaction is associated with two time variables. As seen in the above example, however, each intermediate process originates and terminates with a bare interaction, and consequently

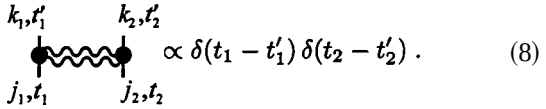 $\propto \delta(t_1-t_1')\,\delta(t_2-t_2')$. (8)

The dressed interaction furthermore depends only on t_2-t_1, for the simple reason that $[(\mathbf{G}^{(1)})_k^j](t_1;t_2)$ depends only on t_2-t_1, for a Hamiltonian with no explicit time dependence [1]. Both δ functions in Eq. (8) and two of the δ functions in Eq. (6) can be omitted if we agree to associate only a single time variable with each vertex. Each vertex retains two spin-orbital indices, however.

To summarize, we consider a perturbative expansion of $\mathbf{G}^{(p)}$ in which the p-particle diagrams consist of quasiparticle ($\mathbf{G}^{(1)}$) lines connected by the dressed interaction in Eq. (8). As usual, unlinked diagrams are excluded from the expansion, as a result of the p-particle generalization [28] of the linked-cluster theorem [29]. The terms *(un)linked* and

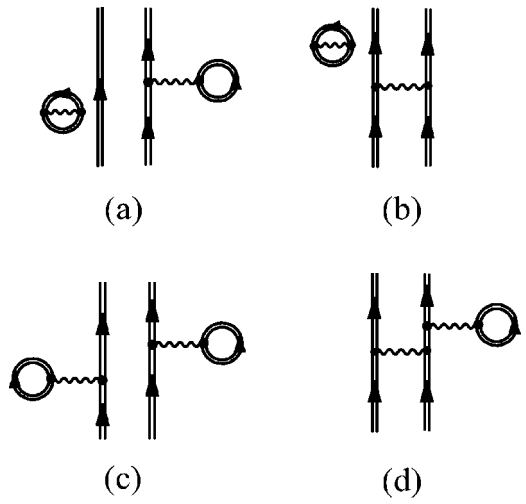

FIG. 1. Two-particle diagrams at second order in $\hat{V}$. Diagrams (a) and (b) are unlinked, diagram (c) is linked but not connected, and (d) is both linked and connected.

(un)connected have various (and occasionally synonymous) meanings in the literature; we follow the convention of Lindgren and Morrison [30]:

Definition 1. A diagram is said to be *connected* if it cannot be separated into pieces without severing an interaction or a propagator line. A diagram is *closed* if it does not contain any incoming or outgoing propagator lines. A diagram that contains a closed, unconnected part is said to be *unlinked*.

An illustration of the distinction between linked and connected diagrams is provided in Fig. 1.

For $p \geqslant 2$ the perturbation series for $\mathbf{G}^{(p)}$ contains terms that are linked but not connected, such as Fig. 1(c) for $p=2$. We denote by $\mathbf{G}_c^{(p)}$ the sum of linked, connected contributions to $\mathbf{G}^{(p)}$, where "c" may equally well stand for "connected" or "cumulant" [31]. We will not consider unconnected diagrams, since the unconnected part $\mathbf{G}^{(p)}-\mathbf{G}_c^{(p)}$ of $\mathbf{G}^{(p)}$ can be recovered, by means of a cumulant expansion, from the propagators $\mathbf{G}^{(n)}$ with $n<p$ [8,9,31,32].

III. CONNECTIVITY AND TOPOLOGY OF DIAGRAMS

nth-(renormalized)-order terms in the expansion of $\mathbf{G}^{(p)}$ are generated from the framework of labeled vertices shown in Fig. 2 by connecting these vertices with p directed $\mathbf{G}^{(1)}$ lines that originate on the vertices labeled $j_1, \ldots, j_p$ and terminate on the vertices $k_1, \ldots, k_p$. A single quasiparticle line should pass through each vertex in the figure, but each line may pass through a different number of vertices. We will not explicitly consider the mixed particle-hole components of $\mathbf{G}^{(p)}$, in which some of the propagator lines originate on a vertex k_μ and terminate at j_λ, because such diagrams can be generated trivially from those described above. Likewise, the p-particle diagrams of time-independent perturbation theory are no different, topologically speaking, than the time-dependent ones, which allows us to apply our results directly to time-independent RDMs; see Sec. VI.

Definition 2. Consider an nth-order term in the expansion of $\mathbf{G}^{(p)}$, constructed from the framework in Fig. 2 as described above. Let $S_m=(j_\lambda, \ldots, k_\mu)$ be the sequence of vertices through which the mth quasiparticle line passes. The *connectivity* of this particular term in the perturbation series is defined to be the set of sequences $\{S_1, \ldots, S_p\}$. The order of the S_m within this set is irrelevant; connectivity is defined only up to permutations of these sequences.

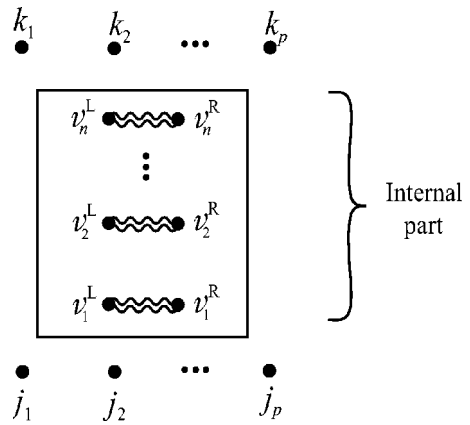

FIG. 2. Framework for constructing nth-(renormalized)-order terms in the expansion of $\mathbf{G}^{(p)}$.

Definition 3. Two p-particle connectivities $\{S_1, \ldots, S_p\}$ and $\{S_1', \ldots, S_p'\}$ are said to be *distinct* if $\{S_1, \ldots, S_p\} \neq \{S_1', \ldots, S_p'\}$ as sets.

The fact that connectivity is defined only up to a permutation of the sequences S_m is a consequence of the antisymmetry of $\mathbf{G}^{(p)}$, whence $(\mathbf{G}^{(p)})^{j_1, \ldots, j_p}_{k_1, \ldots, k_p}$ is unchanged if we permute both $j_\lambda \leftrightarrow j_\mu$ and $k_\lambda \leftrightarrow k_\mu$. This symmetry manifests itself within the perturbation series as the fact that any fully-contracted term from Wick's theorem is unchanged following two such permutations. Self-consistent renormalization—expressing the perturbation series in terms of exact one-particle propagators—does not alter this symmetry.

The "connect-the-dots" paradigm suggested by Fig. 2 provides one method for obtaining all distinct p-particle connectivities. An alternative procedure, advanced by Lande and Smith [33–36], is based upon enumeration of the possible ways in which a given pair of p-particle connectivities can be connected to yield a new p-particle connectivity. While this generates all of the diagrams, it does not do so uniquely, and we shall not employ the Lande-Smith formalism.

Nothing in the definition of connectivity specifies the paths that the quasiparticle lines must take between vertices; as a result of this ambiguity there exist infinitely many diagrammatic representations of the perturbation series. To sort through these various representations it is useful to discuss connectivities as topological objects.

Definition 4. A *diagrammatic presentation* of a connectivity $C=\{S_1, \ldots, S_p\}$ (equivalently, a *diagram* with connectivity C) is an embedding of p lines, with labeled endpoints, as a topological object in three-dimensional space, in which the mth line passes in sequence through the vertices S_m. Once this embedding has been made, all internal vertex labels v_n^{L} and v_n^{R} are deleted.

A connectivity, as defined above, is not a topological object, but topological equivalence of connectivities can be de-

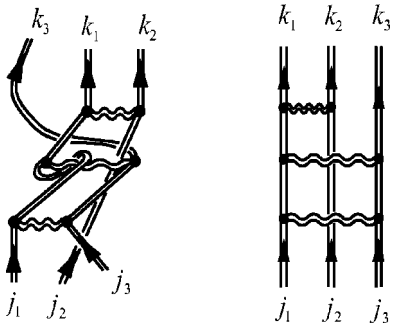

FIG. 3. Two topologically inequivalent embeddings of the same three-particle connectivity.

fined by means of their diagrammatic presentations:

Definition 5. Two p-particle connectivities C_1 and C_2 are said to be *diagrammatically equivalent*, denoted $C_1 \simeq C_2$, if there exist diagrammatic presentations of C_1 and C_2 that are topologically identical (can be deformed into one another in a continuous fashion, without severing any propagator lines or interactions) in three-dimensional space.

Although there are infinitely many diagrams (embeddings) sharing a specified connectivity, in practice it is usually obvious which to choose in order to demonstrate diagrammatic equivalence, namely, the diagram constructed using the shortest possible lines to connect the appropriate vertices. As an example, consider the two diagrams shown in Fig. 3, both of which are embeddings of the connectivity $\{S_1,S_2,S_3\}$, with $S_1=(j_1,v_1^{\mathrm{L}},v_2^{\mathrm{L}},v_3^{\mathrm{L}},k_1)$, $S_2=(j_2,v_3^{\mathrm{R}},k_2)$, and $S_3=(j_3,v_1^{\mathrm{R}},v_2^{\mathrm{R}},k_3)$. Clearly the diagram on the right in Fig. 3 is the preferred choice of embedding. The reader may verify that $\{S_1',S_2',S_3'\}$, where $S_1'=(j_2,v_3^{\mathrm{L}},k_2)$, $S_2'=(j_1,v_1^{\mathrm{L}},v_2^{\mathrm{L}},v_3^{\mathrm{R}},k_2)$, and $S_3'=(j_3,v_1^{\mathrm{R}},v_2^{\mathrm{R}},k_3)$, is distinct from $\{S_1,S_2,S_3\}$ above, but is nevertheless diagrammatically equivalent. The embedding of $\{S_1',S_2',S_3'\}$ shown in Fig. 4 makes this clear.

Given the rules for translating diagrams into algebraic expressions [1,3], it is obvious that if $C_1 \simeq C_2$ then these two connectivities must yield the same algebraic expression. While there may be a large number of distinct connectivities at a given order in perturbation theory, in general each is equivalent to one of a much smaller set of diagrammatically

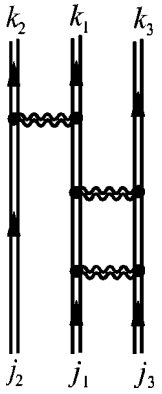

FIG. 4. An embedding of the connectivity $\{S_1',S_2',S_3'\}$ introduced in the text.

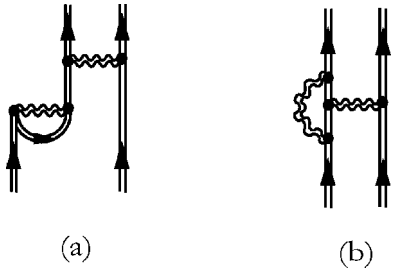

FIG. 5. Diagrams in which v_1^{L} and v_1^{R} are connected by the same quasiparticle line.

inequivalent connectivities. Furthermore, many inequivalent connectivities will differ only by a permutation of the endpoint labels $j_1,\ldots,j_p$ and $k_1,\ldots,k_p$.

Definition 6. Two distinct connectivities $C=\{S_1,\ldots,S_p\}$ and $C'=\{S_1',\ldots,S_p'\}$ are said to be *independent* if the sequences $\{S_m'\}$ cannot be obtained from the sequences $\{S_m\}$ via permutations of the vertex labels $j_1,\ldots,j_p$ and $k_1,\ldots,k_p$.

An equivalent statement of this definition is the following.

Proposition 1. Two connectivities C and C' are not independent if there exist diagrammatic presentations of C and C' that are topologically equivalent when the endpoint labels are deleted.

When connected together, the interaction vertices $\{v_n^{\mathrm{R}}\}$ and $\{v_n^{\mathrm{L}}\}$ in Fig. 2–without the endpoint vertices–make up the *internal part* of the vertex framework. Connectivities that are not independent possess diagrammatically equivalent internal parts, and thus the corresponding algebraic expressions differ only by permutations of $j_1,\ldots,j_p$ and $k_1,\ldots,k_p$. Clearly we need enumerate only the independent diagrams.

Finally, note that explicit self-energy insertions within the quasiparticle lines are forbidden, because we employ exact one-particle propagators in the perturbation series. For example, the diagram in Fig. 5(a) does not appear in the renormalized perturbation series. This does not imply that a single quasiparticle line cannot connect both vertices of the same interaction, but in such cases these vertices must be separated by one or more additional interactions that couple two different quasiparticle lines. An example of this sort is the (allowed) ''vertex correction'' diagram shown in Fig. 5(b). More complicated variants on this theme are of course possible, but the general rule is clear.

Proposition 2. Consider a connectivity $\{S_1,S_2,\ldots\}$ in which the vertices v_n^{L} and v_n^{R} appear within the same sequence, S_m say. This connectivity is forbidden (excluded from the perturbation series) unless v_n^{L} and v_n^{R} are separated within S_m by another vertex $v_n^{\mathrm{L}\prime}$ ($v_n^{\mathrm{R}\prime}$), such that $v_n^{\mathrm{R}\prime}$ ($v_n^{\mathrm{L}\prime}$) is not a member of the sequence S_m.

IV. LADDER-TYPE EXPANSION AND SYMMETRY FACTORS FOR $G_c^{(3)}$

A. Many-particle ladder diagrams

As demonstrated in the preceding section, merely connecting the dots in Fig. 2 to generate distinct nth-order con-

nectivities results in numerous topologically (and therefore algebraically) equivalent connectivities. In this section we will eliminate this redundancy, for three-particle ladder-type diagrams, by introducing a well-defined algorithm that accounts for all nth-order connectivities possessing a ladder-type embedding. In addition, this algorithm automatically accounts for connectivities such as the one shown in Fig. 6, which might not immediately appear to be ladder diagrams but are nonetheless equivalent to more traditional-looking three-particle ladders.

First let us define precisely what is meant by a ladder connectivity.

Definition 7. A p-particle connectivity is called a *p-particle ladder* if it possesses a connected diagrammatic presentation in which (i) the interactions do not overlap with one another in time (that is, in the vertical direction), and (ii) no quasiparticle lines run backward in time.

The presentations in Figs. 4 and 6 clearly satisfy this definition. Examples of nonladder diagrams include vertex corrections such as

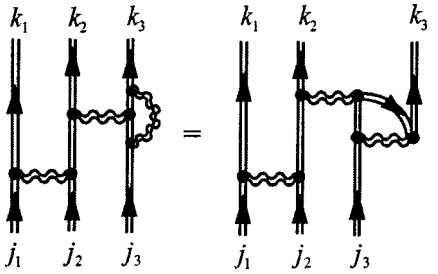

(9)

and particle-hole scattering diagrams such as

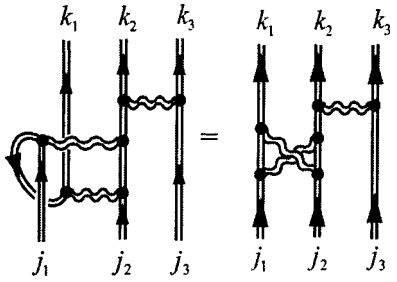

(10)

Whereas p-particle ladder diagrams involve only simultaneous two-body correlations, other types of diagrams involve three body and higher correlations [19], and should therefore be less significant in molecular electronic structure applications. In what follows, we restrict our discussion to ladder diagrams only.

B. Construction of the three-particle ladders

A slight modification of the vertex framework introduced previously yields a counting algorithm for the three-particle ladders. This modified framework is shown in Fig. 7(a) and consists again of n time-ordered interactions. For clarity we have not included the vertex labels $\{v_n^{\mathrm{R}}\}$ and $\{v_n^{\mathrm{L}}\}$ in this figure, but we assume that the vertices are labeled as in Fig. 2. The interactions are drawn horizontally so that they do not overlap in time. Let t_λ^R and t_λ^{L} be the time arguments associated with the vertices v_λ^{R} and v_λ^{L}, respectively. Ladders constructed from Fig. 7 are assumed to be time ordered such that

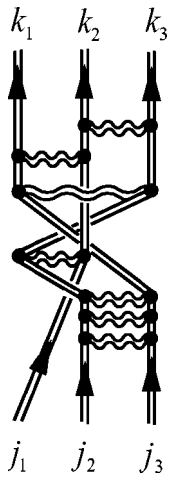

FIG. 6. A three-particle ladder diagram.

$$t_1^{\mathrm{A}_1} < t_1^{\mathrm{A}_1'} < t_2^{\mathrm{A}_2} < t_2^{\mathrm{A}_2'} < \cdots < t_n^{\mathrm{A}_n} < t_n^{\mathrm{A}_n'}, \tag{11}$$

where each $\mathrm{A}_\lambda, \mathrm{A}_\lambda' \in \{\mathrm{R},\mathrm{L}\}$. The necessity of this time order follows immediately from *Definition 7*; while the relative time order of v_λ^{R} and v_λ^{L} is unspecified, these vertices must be separated in time from all other interactions, else the result is not a ladder diagram. As a practical matter, this means that we consider only topological deformations that preserve the time order of the interactions. We shall return to this point at the end of Sec. V.

Construction of three-particle ladder diagrams begins, as shown in Fig. 7(a), by drawing three quasiparticle lines extending from the vertices j_1, j_2, and j_3 to three of the interaction vertices. For generality, the quasiparticle line originating at j_1 is attached to v_m^{L}, with $2 \leqslant m \leqslant n$. The case where this line attaches to v_m^{R} will be considered separately.

We have less freedom, within the ladder approximation, to attach the remaining two quasiparticle lines, because given the arrangement in Fig. 7 no quasiparticle line may run backward in time, else the resulting diagram will not be a ladder. Hence the remaining two quasiparticle lines must attach to v_1^{L} and v_1^{R}.

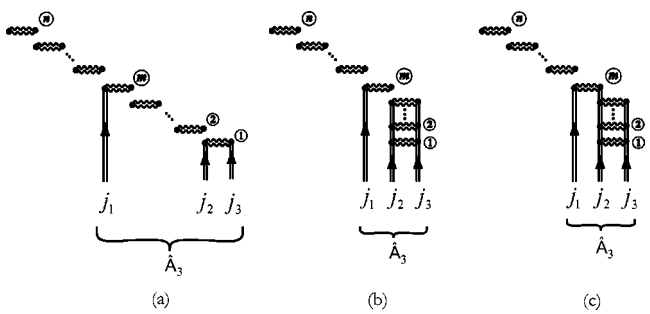

FIG. 7. Diagrammatic representations of various steps in the algorithmic construction of nth-order, three-particle ladders. See the text for an explanation of each step.

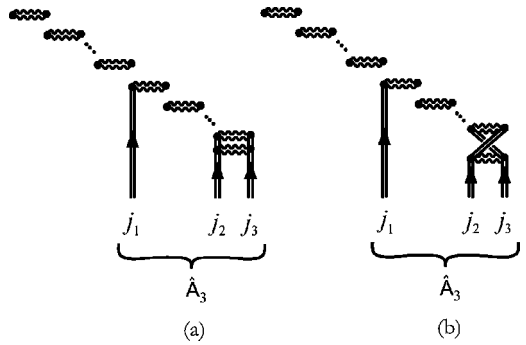

FIG. 8. (a) Untwisted and (b) twisted connection of the second interaction in Fig. 7(a).

We refer to partially-connected frameworks, such as those shown in Figs. 7(a)–7(c), as *nascent connectivities*. Starting from the nascent connectivity in Fig. 7(a), we intend to buildup the internal part in a systematic manner that accounts for all topologically equivalent possibilities each time another interaction is appended. This procedure is carried out graphically, meaning that we have made an implicit choice of embedding for each connectivity. Consequently, within the constructive algorithms presented in this section and in Sec. V, the concept of diagrammatic equivalence is the same as the notion of topological equivalence in three-dimensional space.

For each nth-order internal part constructed by our algorithm, every permutation of the labels j_1, j_2, and j_3 yields a distinct connectivity. We account for these six nonindependent connectivities with an operator $\hat{\mathsf{A}}_3$, as indicated in Fig. 7, where $\hat{\mathsf{A}}_p$ is defined as the sum over signed permutations of $\{j_1, \ldots, j_p\}$. For later use let us define $\hat{\mathsf{A}}'_p$ to be the sum over signed permutations of $\{k_1, \ldots, k_p\}$. The presence of $\hat{\mathsf{A}}_3$ in Fig. 7 compensates for our arbitrary choice of labels for the three incoming quasiparticle lines.

The next step in the counting algorithm is to extend the j_2 and j_3 quasiparticle lines in order to incorporate interactions 2 through $(m-1)$. Each of these interactions must be appended to the nascent connectivity in order, for otherwise there is no way to complete the connectivity without backward-propagating quasiparticle lines. Each interaction can, however, be connected to the one beneath it in two different ways, one twisted and one untwisted. These possibilities are illustrated, for the second interaction, in Fig. 8.

The untwisted nascent connectivity, Fig. 8(a), is a diagrammatic presentation of $\{S_1, S_2, S_3\}$ with

$$S_1 = (j_1, v_m^{\mathrm{L}}, \ldots), \tag{12a}$$

$$S_2 = (j_2, v_1^{\mathrm{L}}, v_2^{\mathrm{L}}, \ldots), \tag{12b}$$

$$S_3 = (j_3, v_1^{\mathrm{R}}, v_2^{\mathrm{R}}, \ldots). \tag{12c}$$

The twisted variant, Fig. 8(b), has nascent connectivity $\{S'_1, S'_2, S'_3\}$, with

$$S'_1 = (j_1, v_m^{\mathrm{L}}, \ldots), \tag{13a}$$

$$S'_2 = (j_2, v_1^{\mathrm{L}}, v_2^{\mathrm{R}}, \ldots), \tag{13b}$$

$$S'_3 = (j_3, v_1^{\mathrm{R}}, v_2^{\mathrm{L}}, \ldots). \tag{13c}$$

For any connectivity, the interchange $v_m^{\mathrm{L}} \leftrightarrow v_m^{\mathrm{R}}$ leads to a distinct but diagrammatically (that is, topologically) equivalent connectivity. Consequently, if one completes each pair of sequences S_m and S'_m in exactly the same fashion, the resulting connectivities will be diagrammatically equivalent up to a permutation of j_2 and j_3. That is,

$$\{S_1, S_2, S_3\} \simeq (j_2\ j_3)\{S'_1, S'_2, S'_3\}, \tag{14}$$

where $(j_2\ j_3)$ denotes the transposition operator for j_2 and j_3.

Taking into account all nonindependent connectivities that can be generated from $\{S_1, S_2, S_3\}$ and $\{S'_1, S'_2, S'_3\}$ via permutations of the endpoint labels, one sees that these connectivities show up in the perturbation series as $\hat{\mathsf{A}}_3\ \hat{\mathsf{A}}'_3\{S_1, S_2, S_3\}$ and $\hat{\mathsf{A}}_3\ \hat{\mathsf{A}}'_3\{S'_1, S'_2, S'_3\}$. Since

$$\hat{\mathsf{A}}_3\ \hat{\mathsf{A}}'_3((j_2\ j_3)\{S'_1, S'_2, S'_3\}) \simeq \hat{\mathsf{A}}_3\ \hat{\mathsf{A}}'_3\{S'_1, S'_2, S'_3\}, \tag{15}$$

each complete connectivity generated from the nascent one in Fig. 8(b) is topologically equivalent to a connectivity obtained from Fig. 8(a). [We emphasize, however, that connectivities generated from 8(a) and 8(b) are distinct, in the sense of *Definition 3*.] As a result of this equivalence we may discard connectivities generated from Fig. 8(b), substituting instead a multiplicative symmetry factor of 2 associated with Fig. 8(a).

This result clearly generalizes to interactions $3, \ldots, (m-1)$ in Fig. 7, since each must be attached to the j_2 and j_3 quasiparticle lines. Thus the untwisted ladder framework, obtained by connecting these interactions and depicted in Fig. 7(b), carries an overall symmetry factor of 2^{m-2}.

Next we must attach the mth interaction to the j_2-j_3 ladder. The free vertex v_m^{R} of the mth interaction may be attached to either the left or the right side of this ladder, with the former choice shown in Fig. 7(c). In the case that this interaction is attached to the right side of the ladder—which generates an entirely distinct set of connectivities—the resulting framework is topologically equivalent to Fig. 7(c) following a permutation of j_2 and j_3. Arguing as before, a factor of two accounts for the possibility of attaching v_m^{R} to the right side of the j_2-j_3 ladder. Hence the symmetry factor associated with the nascent connectivity in Fig. 7(c) is 2^{m-1}.

It is convenient to backtrack at this point, in order to consider the case where the quasiparticle line labeled "j_1" is connected to v_m^{R} rather than v_m^{L}. Obviously this does not affect construction of the j_2-j_3 ladder in Fig. 7(b), yet a distinct collection of connectivities is obtained because S_1 in this case is given by $S_1 = (j_1, v_m^{\mathrm{R}}, \ldots)$ rather than $S_1 = (j_1, v_m^{\mathrm{L}}, \ldots)$ [cf. Eqs. (12a) and (13a)]. Again, though, the resulting nascent connectivity through m interactions is

FIG. 9. All independent third-order, three-particle ladders.

topologically equivalent to the one in Fig. 7(c) and can be neglected by increasing the symmetry factor for Fig. 7(c) to 2^m.

It remains to connect the final $(n-m)$ interactions, starting with the $(m+1)$st. There are $\binom{3}{2}$ pairs of vertices to which we might attach each given interaction and two possible ways to make this connection, one twisted and one untwisted. By now it should be clear that the twisted variants can be neglected if we multiply their untwisted counterparts by a factor of 2 for each interaction. The set of untwisted diagrams is, by construction, precisely the set of all diagrammatically distinct three-particle ladders. The remaining $n-m$ interactions contribute a factor of 2^{n-m} to the symmetry coefficient, resulting in an overall symmetry factor of $2^m \times 2^{n-m}=2^n$ for each diagrammatically distinct, nth-order ladder. Note that this result is independent of the index m where the j_1 quasiparticle line was originally attached.

Finally, an antisymmetrizer $\hat{\mathsf{A}}_3'$ must be included to permute k_1, k_2, and k_3, since the definition of a ladder involves only the internal part of the connectivity and says nothing about the manner in which this internal part connects to the endpoint vertices. Hence the sum of all nth-order ladder diagrams in the expansion of $\mathbf{G}_c^{(3)}$ is equal to the action of $2^n\hat{\mathsf{A}}_3\,\hat{\mathsf{A}}_3'$ on the sum of independent three-particle ladders, and we have our desired symmetry coefficient.

An ancillary result that follows from the above algorithm is the precise number of independent three-particle ladders. Observe that $\binom{3}{2}^{n-m}$ distinct internal connectivities can be generated from the nascent connectivity in Fig. 7(c). Summation over possible values of m yields the number of independent ladders at nth order

$$\sum_{m=2}^{n}\binom{3}{2}^{n-m}=\frac{1}{2}(3^{n-1}-1), \tag{16}$$

which is valid for $n\geqslant 2$. (There are no first-order, three-particle ladders because a ladder must be connected, by definition.) In a sense, the precise number of ladder diagrams is not so important, since we now possess and algorithm that

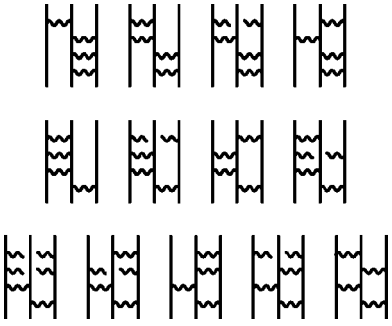

FIG. 10. All independent fourth-order, three-particle ladders.

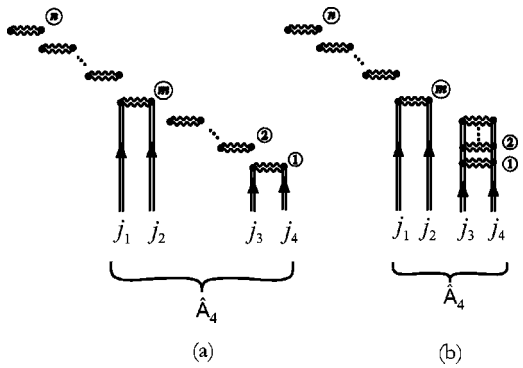

FIG. 11. Steps in the four-particle counting algorithm (first case). See the text for an explanation of each step.

generates them without redundancies. However, this number is a useful check that the algorithm has been employed correctly.

For the reader's convenience, we restate the main results of this section.

Theorem 1. At nth order in the dressed interaction, there exist $(3^{n-1}-1)/2$ independent three-particle ladder connectivities (that is, ladders that are diagrammatically inequivalent when unlabeled). Each is diagrammatically equivalent to 2^n distinct ladder connectivities in the $\mathbf{G}_c^{(3)}$ perturbation series. The total contribution to $\mathbf{G}_c^{(3)}$ from nth-order ladders equals $2^n\hat{\mathsf{A}}_3\,\hat{\mathsf{A}}_3'$ acting on the sum of independent three-particle ladders.

As an illustration, we present in Figs. 9 and 10 all of the independent three-particle ladders at third and fourth order, respectively, in the order that they are generated by the algorithm described in this section. For conciseness these diagrams are drawn using single lines, which clearly does not affect their topology.

With the machinery developed in this section we can also derive the symmetry coefficient for two-particle ladders. Actually this is very simple because there are only two possible ways to append each successive interaction, one twisted and another untwisted. The result is given in the following proposition.

Proposition 3. The total contribution to $\mathbf{G}_c^{(2)}$ from nth-order ladders equals $2^{n-1}\hat{\mathsf{A}}_2\,\hat{\mathsf{A}}_2'$ acting on the lone diagrammatically inequivalent two-particle ladder.

V. LADDER-TYPE EXPANSION AND SYMMETRY FACTORS FOR $\mathbf{G}_c^{(4)}$

A. First case

Construction of the four-particle ladders proceeds along similar lines, but there are two cases to consider. Starting from a sequence of n time-ordered interactions, one must again attach two quasiparticle lines (labeled j_3 and j_4, say) to the first of these, while the remaining two quasiparticle lines (labeled j_1 and j_2) may be attached arbitrarily. We first consider the case where these two lines are attached to the same interaction, say the mth, where $2\leqslant m<n$. This nascent connectivity is shown in Fig. 11(a). Note that m must be

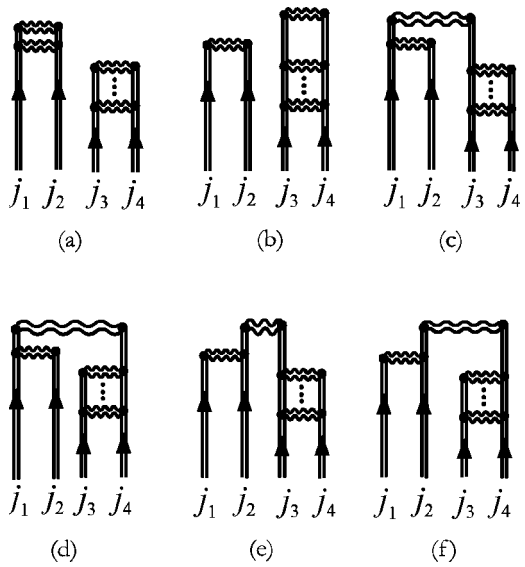

FIG. 12. Possible nascent connectivities associated with connecting the first $(m+1)$ interactions in Fig. 11(b).

strictly less than n in this case, because when $m=n$ there is no way to build a connected diagram without backward-propagating quasiparticle lines. Analogous to the three-particle case, we indicate a sum over signed permutations of $j_1, \ldots, j_4$ with the operator $\hat{\mathsf{A}}_4$; this antisymmetrization justifies our arbitrary choice of quasiparticle labels.

The next step is to buildup a ladder sequence from the first $(m-1)$ interactions, just as we did in the three-particle construction. The resulting framework is shown in Fig. 11(b) and carries a symmetry factor of 2^{m-2} to account for twists within the ladder.

We now come to the mth interaction. There are $\binom{4}{2}$ pairs of vertices to which we may attach this interaction; as usual we include a factor of 2 in each case and thereby consider only connectivities that are untwisted through the first $m+1$ interactions. There are six such, as shown in Fig. 12. The latter four are seen to be permutations of a single nascent connectivity, while the other two are unconnected. Through the first $(m+1)$ interactions, then, all distinct four-particle ladder connectivities are diagrammatically equivalent to either (a), (b), or (c) in Fig. 12. Diagrams 12(a) and 12(b) each carry a symmetry factor of $2^{(m-1)}$, while the coefficient for 12(c) is $2^{(m+1)}$, where the extra factor of 4 accounts for the topologically equivalent connectivities in Figs. 12(d)–12(f).

Any diagram generated from Fig. 12(c) is necessarily connected. Untwisted connection of the remaining $(n-m-1)$ interactions exhausts all inequivalent connectivities that can be built from Fig. 12(c), while a factor of 2^{n-m-1} accounts for the equivalent, twisted connectivities. The overall symmetry factor for independent ladders constructed from Fig. 12(c) is $2^{n-m-1}\times 2^{m+1}=2^n$, independent of m.

The situation is somewhat different for the as-yet-unconnected possibilities in Figs. 12(a) and 12(b). Appending the $(m+2)$nd interaction to either of these nascent connectivities results in a set of six diagrams analogous to those in Fig. 12. Two of these each consist of a pair of unconnected ladders, while the other four are connected and also topologically equivalent. The four connected diagrams can be treated as above, the result being a symmetry factor of 2^n once the connectivity has been completed. For the two unconnected diagrams, attaching the $(m+3)$rd interaction leads to another six possibilities, and so on, until finally we come to attach the nth interaction. This must be done in such a way that the entire diagram becomes connected, so we have in this final case only the four topologically equivalent, connected possibilities analogous to Figs. 12(c)–12(f). As with the other cases the result is a symmetry coefficient of 2^n for each completed connectivity.

To obtain the number of independent four-particle ladders, in the case that all four propagator lines initially connect to only two interaction rungs, let q index the interaction at which the j_1-j_2 and j_3-j_4 halves of the diagram become connected $[(m+1)\leqslant q\leqslant n]$. For example, $q=(m+1)$ in Fig. 12(c) but connectivities built from Figs. 12(a) and 12(b) do not become connected until some $q>(m+1)$. A diagram that becomes connected at the qth interaction ultimately generates $\binom{4}{2}^{n-q}$ topologically inequivalent ladder diagrams.

Two of the nascent connectivities in Fig. 12 are unconnected through the first m interactions, and the number of unconnected nascent connectivities doubles each time another interaction is appended. Hence there are 2^{q-m-1} topologically inequivalent nascent connectivities that first become connected at the qth interaction. Summation over the possible values for q and m yields the number of independent four-particle ladders for the case discussed thus far:

$$\sum_{m=2}^{n-1}\sum_{q=m+1}^{n} 2^{q-m-1}\binom{4}{2}^{n-q} = \frac{3}{10}(6^{n-2}-1)-\frac{1}{2}(2^{n-2}-1), \qquad (17)$$

for each $n\geqslant 3$.

B. Second case

There is a second case to consider, namely, that in which the j_1 and j_2 quasiparticle lines do not initially connect to the same interaction. (The j_3 and j_4 interactions must still attach to v_1^{L} and v_1^{R}.) A framework for discussing this case is depicted in Fig. 13. We attach the j_1 line to v_r^{L} and the j_2 line to v_m^{L}, for $2\leqslant m<r\leqslant n$. Cases where $m>r$ amount to a permutation of j_1 and j_2, and the operator $\hat{\mathsf{A}}_4$ indicated in Fig. 13 accounts for all such permutations. Cases in which the j_1 line, the j_2 line, or both attach at the right of an interaction will be incorporated as we proceed.

Through $(r-1)$ interactions, the four-particle nascent connectivity in Fig. 13 is the same as a three-particle nascent connectivity that was considered previously, in Fig. 7(a). (The fact that the endpoint labels differ is unimportant since we consider all permutations of these labels.) The results of Sec. IV B thus furnish the appropriate symmetry coefficient through $(r-1)$ interactions, namely 2^{r-1}. By construction, this factor accounts for all diagrammatically equivalent nascent connectivities, so we may assume that the first $r-1$ interactions in Fig. 13 are connected without topological re-

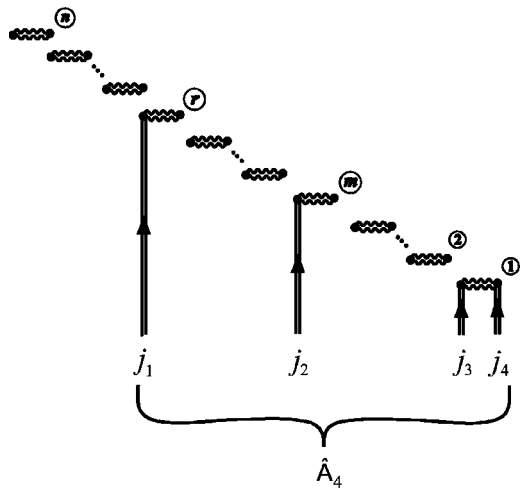

FIG. 13. Illustration of the four-particle counting algorithm (second case).

dundancies. As a result, each of the $\binom{3}{2}$ ways in which the rth interaction can be connected to those below it generates a topologically distinct nascent connectivity. An additional factor of 2 accounts for the fact that we might have attached the j_1 propagator line to v_r^{R}, which generates exactly the same set of diagrams as when this propagator attaches to v_r^{L}. Finally, the remaining $n-r$ interactions can each be attached in $\binom{4}{2}$ ways, with the usual factor of 2 at each interaction to account for the twisted connectivities. The total symmetry coefficient is thus $2^{r-1}\times 2\times 2^{n-r}=2^n$, just as it was in the other four-particle case.

The total number of ladder diagrams for this case is obtained as follows. We know that nascent four-particle ladders generated from Fig. 13 look just like three-particle ladders, through the $(r-1)$st interaction, so Eq. (16) tells us that there are $(3^{r-2}-1)/2$ nascent four-particle ladders through the first $(r-1)$ interactions. [In using Eq. (16), we have summed over possible values of m from 2 to $(r-1)$, hence this result is independent of m.] Appending the rth interaction increases the number of diagrams by a factor of $\binom{3}{2}$, but following this each additional interaction increases the number of topologically inequivalent diagrams by a factor of $\binom{4}{2}$. The number of independent four-particle ladders in this second case is therefore

$$\sum_{r=3}^{n}\frac{1}{2}(3^{r-2}-1)\binom{3}{2}\binom{4}{2}^{n-r}$$
$$=\left(\frac{3^{(n-1)}}{2}\right)(2^{n-2}-1)-\frac{3}{10}(6^{n-2}-1), \quad (18)$$

for each $n\geqslant 3$. Combining this with Eq. (17), we summarize our results for four-particle ladders in the following Theorem.

Theorem 2. At nth order there exist $(2^{n-2}-1)(3^{n-1}-1)/2$ independent, four-particle ladders. The total contribution to $\mathbf{G}_c^{(4)}$ from nth-order ladders equals $2^n\hat{\mathrm{A}}_4\,\hat{\mathrm{A}}_4'$ acting on the sum of these independent ladder diagrams.

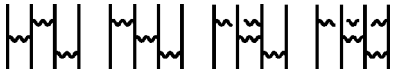

FIG. 14. All independent four-particle ladders at third order.

As an illustration of these results, the independent four-particle ladders at third order are depicted in Fig. 14, in the order in which they are generated by the construction described above. The first of these diagrams belongs to case 1 while the other three arise from case 2.

At fourth order there are 39 independent ladder connectivities. We shall not depict all of these, but two are shown in Fig. 15 in order to illustrate a subtle point that does not arise until fourth order. As indicated by Eq. (11), our ladder diagrams are constructed with an intrinsic time order, since we do not consider topological deformations that alter the time order of the interactions. Consequently, the procedure described in this section generates both of the diagrams shown in Fig. 15, which differ only in the relative time order of the final two interactions. In evaluating the diagram shown in Fig. 15(a), for example, the time arguments t_4^{R} and t_4^{L} for the topmost interaction are restricted to be greater than either t_3^{R} or t_3^{L}, the time arguments for the interaction below. This is no problem in practice, and in fact both diagrams in Fig. 15 are easily combined into a single diagram by combining the two time integration ranges. Our restriction on time order merely simplifies the algorithm for constructing the ladders and does not affect the symmetry factors.

VI. LADDER-TYPE DECOUPLING APPROXIMATIONS

In this section we give an overview of how the formalism developed herein can be applied to derive decoupling approximations for the three- and four-particle propagators or RDMs, within a renormalized ladder-type approximation. As we have indicated, the validity of such an approximation depends upon simultaneous three-body correlations being small, although it has recently been shown [19] that self-consistent iteration of the contracted Schrödinger equation serves to rebuild three-body correlations that are neglected by ladder-type decoupling approximations for the 3- and 4-RDMs. At any rate, our intention here is not to justify this approximation but rather to demonstrate how the results presented in Secs. IV and V greatly facilitate derivation of the appropriate decoupling formulas.

The connected part of the two-particle propagator, which we represent diagrammatically as

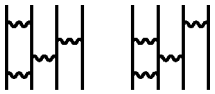

(a) (b)

FIG. 15. Two independent four-particle ladders that differ only in time order.

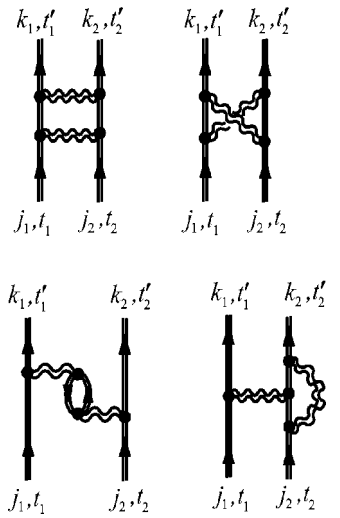

FIG. 16. A few diagrams in the expansion of $\mathbf{G}_c^{(2)}$, at second order in the dressed interaction.

$$i^2\left[(\mathbf{G}_c^{(2)})_{k_1,k_2}^{j_1,j_2}\right](t_1,t_2;t_1',t_2') = \quad , \tag{19}$$

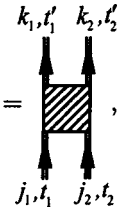

possesses a perturbative expansion consisting of connected two-particle diagrams, several of which are shown in Fig. 16. Likewise, $\mathbf{G}_c^{(p)}$ can be expanded in terms of connected p-particle diagrams. To develop decoupling approximations for $\mathbf{G}_c^{(3)}$ and $\mathbf{G}_c^{(4)}$ in terms of $\mathbf{G}_c^{(2)}$, we take the latter to be a known quantity and recast the perturbation series for $\mathbf{G}_c^{(3)}$ and $\mathbf{G}_c^{(4)}$ as expansions in an effective interaction equal to the sum of all connected two-particle diagrams; this is precisely the interaction shown diagrammatically in Eq. (19).

Consider the selection of connected three-particle diagrams in Fig. 17. (Endpoint labels have been omitted in this figure, for clarity; all diagrams are assumed to be labeled in the same way.) Up to permutations of the endpoint labels, each is contained within the single renormalized diagram

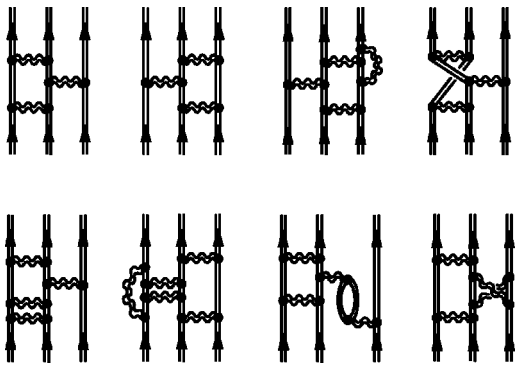

FIG. 17. Selected diagrams in the expansion of $\mathbf{G}_c^{(3)}$.

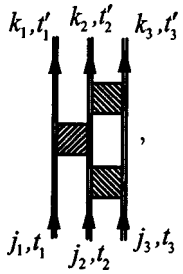

in which the hatched square is the same effective interaction that appears in $\mathbf{G}_c^{(2)}$. The veracity of this claim may be verified by substituting various two-particle diagrams (Fig. 16) in place of the effective interaction. We call this diagram a *quasipair ladder* (QPL) [26] because the effective interaction, according to Eq. (19), represents the complete interaction between a *pair* of correlated *quasi*particles within the many-body medium. In each of the diagrams shown in Fig. 17, the interactions can be partitioned into three groups that do not overlap in time, corresponding to the three effective interactions in the above QPL diagram.

The diagram rules and symmetry coefficients derived previously must be modified slightly in order to account for this latest renormalization. In contrast to the dressed interaction discussed in Sec. II, the effective interaction in Eq. (19) is nonlocal in all four of its time arguments, so there is no analogue of Eq. (8) for this interaction. As a result, we must introduce an additional caveat: repeated factors of this effective interaction between the same two quasiparticle lines are forbidden. This eliminates certain of the diagrams generated in Secs. IV and V.

The symmetry factors derived previously are also modified following the renormalization introduced in this section. Because $\mathbf{G}_c^{(2)}$ is an antisymmetric function of its coordinates, and since no coordinate permutations are included in Eq. (19), the effective interaction must carry this antisymmetry. However, symmetry factors derived in Secs. IV and V pertained to an interaction that was not antisymmetrized. To adapt these for use in the present case, the nth-order symmetry coefficient of 2^n must be divided by 4^n in order to account for the four distinct coordinate permutations (think of them as twisted diagrams) contained within each factor of the effective interaction.

Eliminating the forbidden diagrams from Figs. 9 and 10, and supplementing the lone second-order ladder diagram, one obtains the three-particle QPL diagrams shown in Fig. 18. In light of the remarks above, the appropriate symmetry factor for each is $(1/2)^n$, where n is the number of effective interactions. When augmented by this factor and also permutations of the endpoint labels, the diagrams in Fig. 18 provide either a second-, third-, or fourth-order QPL approximation to $\mathbf{G}_c^{(3)}$. Similar QPL approximations for $\mathbf{G}_c^{(4)}$ follow from the diagrams and symmetry factors derived in Sec. V.

The effective interaction appearing in the QPL diagrams can be obtained, in terms of $\mathbf{G}_c^{(2)}$, by inverting the integral equation corresponding to Eq. (19), which allows the QPL

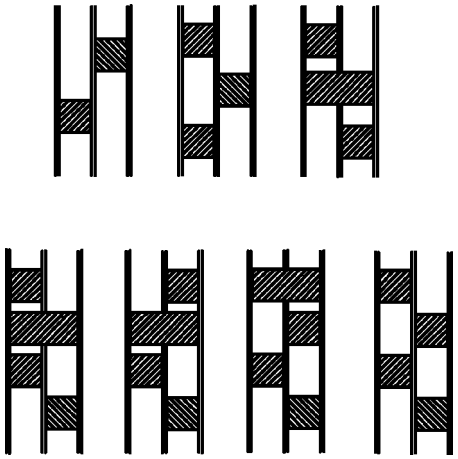

FIG. 18. Three-particle QPL diagrams, through fourth order.

diagrams to be evaluated in terms of $\mathbf{G}_c^{(2)}$. In conjunction with known expressions [8,9,31,32] for the unconnected contributions to the propagators, QPL estimates of $\mathbf{G}_c^{(3)}$ and $\mathbf{G}_c^{(4)}$ thus provide a *reconstruction* of $\mathbf{G}^{(3)}$ and $\mathbf{G}^{(4)}$, as functionals of $\mathbf{G}^{(2)}$. These functionals can be used to express the propagator equations of motion in terms of $\mathbf{G}^{(2)}$ alone.

As noted previously, time-independent many-body perturbation theory shares a common diagrammatic representation with the time-dependent theory (from which the time-independent theory is obtained, as a limiting case), although the rules for evaluating these diagrams (time integration versus energy denominators, etc.) obviously differ. The derivations in Secs. IV and V, however, utilized only the topological properties of the diagrams and, implicitly, their relation to Wick's theorem, so all of these results are equally valid for time-independent diagrams. In particular, one can define a QPL approximation for the 3- and 4-RDMs using exactly the same diagrams as those appearing in the time-dependent QPL approximation. An approximate decoupling procedure can then be introduced [16,22,26], by means of which the time-independent three- and four-particle diagrams are written as matrix products of two-particle pieces that are readily evaluated in terms of the 2-RDM.

The procedure described above has been implemented by Nakatsuji and Yasuda [21,22] to obtain *reconstruction functionals* for the 3- and 4-RDMs; such functionals are needed in order to solve the contracted Schrödinger equation directly for the 2-RDM. Nakatsuji and Yasuda consider only the lowest-order (second-order) correction to the 3-RDM and utilize an unconnected approximation for the 4-RDM. The symmetry coefficients for their second-order, three-particle QPL approximation appear to have been derived by brute-force enumeration of the diagrams, since no mention is made of any systematic paradigm. The procedures developed herein thus simplify the derivation of Nakatsuji and Yasuda's reconstruction functionals. More importantly, our methods allow this ''reconstructive'' perturbation theory to be extended to higher orders, and to the 4-RDM as well as the 3-RDM, with relatively little effort. These extensions are discussed more fully in Ref. [26].

VII. SUMMARY

We have discussed diagrammatic representations of the perturbation series for many-particle propagators, in terms of connectivities and their topology. For many-particle propagators, it is vital to have in one's mind a clear and precise understanding of the relationship between diagrams and distinct terms in the perturbation series, because there are numerous, topologically inequivalent ways to embed a *p*-particle diagram as a topological object in three-dimensional space. In addition, many terms in the perturbation series possess the same diagrammatic embedding.

With regard to the latter point, we have studied in detail the connected, ladder-type diagrams arising in the expansions of the three- and four-particle propagators $\mathbf{G}^{(3)}$ and $\mathbf{G}^{(4)}$. Symmetry coefficients (diagram weights) were derived, which account for the number of distinct connectivities (terms in the perturbation series) that are manifested in each topologically distinct diagram. Use of these symmetry coefficients allows the perturbation series to be limited to inequivalent diagrams, for a savings of 2^n diagrams at nth order. (Notably, this coefficient differs from the diagram weight for two-particle ladder diagrams, another indication that three- and four-particle diagrams have more complicated topologies that one- or two-particle diagrams.) Finally, algorithms were introduced that generate the necessary sets of inequivalent three- and four-particle ladder diagrams exactly, without omissions or redundancies.

Expansions of $\mathbf{G}^{(3)}$ and $\mathbf{G}^{(4)}$ in terms of a renormalized pair interaction derivable from $\mathbf{G}^{(2)}$ allows for a self-consistent decoupling of the various hierarchies of propagator and RDM equations of motion, thus providing a scheme for direct determination of either $\mathbf{G}^{(2)}$ or the 2-RDM. Absent some systematic procedure, direct enumeration of all necessary diagrams is laborious and prone to error, due to the complicated topology of three- and four-particle diagrams. Equipped with the algorithms and symmetry coefficients introduced herein, however, derivation of the decoupling formulas is quite facile.

This methodology is extendible, in principle, to many-particle diagrams that are not of the ladder variety, although the author's experience hints that the formalism is more complicated for nonladder diagrams. These extensions are worth pursuing, should the ladder-type decoupling schemes outlined in Sec. VI yield a useful starting point for direct calculation of two-particle propagators or RDMs.

ACKNOWLEDGMENTS

The author thanks Professor John Harriman for extensive discussions and for comments on the manuscript. This work was financially supported by the U.S. Department of Defense.

[1] A. L. Fetter and J. D. Walecka, *Quantum Theory of Many-Particle Systems* (McGraw-Hill, New York, 1971).
[2] G. Csanak, H.S. Taylor, and R. Yarris, Adv. At. Mol. Phys. **7**, 287 (1971).
[3] R. D. Mattuck, *A Guide to Feynman Diagrams in the Many-Body Problem*, 2nd ed. (McGraw-Hill, New York, 1976).
[4] P. Jørgensen and J. Simons, *Second Quantization-Based Methods in Quantum Chemistry* (Academic, New York, 1981).
[5] Y. Öhrn and G. Born, Adv. Quantum Chem. **13**, 1 (1981).
[6] P.C. Martin and J. Schwinger, Phys. Rev. **115**, 1342 (1959).
[7] L. P. Kadanoff and G. Baym, *Quantum Statistical Mechanics* (Benjamin, New York, 1962).
[8] C. de Dominicis and P.C. Martin, J. Math. Phys. **5**, 14 (1964).
[9] C. de Dominicis and P.C. Martin, J. Math. Phys. **5**, 31 (1964).
[10] R.D. Mattuck and A. Theumann, Adv. Phys. **20**, 721 (1971).
[11] S. Fujita, Kinam **5**, 234 (1983).
[12] S.-J. Wang, W. Zuo, and W. Cassing, Nucl. Phys. A **573**, 245 (1994).
[13] H. Nakatsuji, Phys. Rev. A **14**, 41 (1976).
[14] S.-J. Wang and W. Cassing, Ann. Phys. (N.Y.) **159**, 328 (1985).
[15] V.A. Golovko, Physica A **230**, 658 (1996).
[16] K. Yasuda, Phys. Rev. A **59**, 4133 (1999).
[17] D. Mukherjee and W. Kutzelnigg, J. Chem. Phys. **114**, 2047 (2001); **114**, 8226(E) (2001).
[18] J.M. Herbert and J.E. Harriman, Phys. Rev. A **65**, 022511 (2002).
[19] J. M. Herbert and J. E. Harriman, J. Chem. Phys. **117**, 7464 (2002).
[20] F. Colmenero and C. Valdemoro, Int. J. Quantum Chem. **51**, 369 (1994).
[21] H. Nakatsuji and K. Yasuda, Phys. Rev. Lett. **76**, 1039 (1996).
[22] K. Yasuda and H. Nakatsuji, Phys. Rev. A **56**, 2648 (1997).
[23] D.A. Mazziotti, Phys. Rev. A **57**, 4219 (1998).
[24] H. Nakatsuji, in *Many-Electron Densities and Reduced Density Matrices*, edited by J. Cioslowski (Plenum, New York, 2000), p. 85.
[25] C. Valdemoro, L.M. Tel, E. Pérez-Romero, and A. Torre, J. Mol. Struct.: THEOCHEM **537**, 1 (2001); **574**, 255(E) (2001).
[26] J. M. Herbert (unpublished).
[27] O. Sinanoğlu, J. Chem. Phys. **36**, 706 (1962).
[28] D.H. Kobe, J. Math. Phys. **7**, 1806 (1966).
[29] J. Goldstone, Proc. R. Soc. London, Ser. A **239**, 267 (1957).
[30] I. Lindgren and J. Morrison, *Atomic Many-Body Theory*, 2nd ed. (Springer-Verlag, Berlin, 1986).
[31] P. Ziesche, in *Many-Electron Densities and Reduced Density Matrices*, edited by J. Cioslowski (Plenum, New York, 2000), p. 33.
[32] D.A. Mazziotti, Chem. Phys. Lett. **289**, 419 (1998).
[33] A. Lande and R.A. Smith, Phys. Lett. **131B**, 253 (1983).
[34] R. A. Smith, in *Condensed Matter Theories*, edited by F. B. Malik (Plenum, Berlin, 1986), Vol. 1, p. 9.
[35] R. A. Smith and A. Lande, in *Condensed Matter Theories*, edited by J. S. Arponen, R. F. Bishop, and M. Manninen (Plenum, New York, 1988), Vol. 3, p. 1.
[36] A. Lande and R.A. Smith, Phys. Rev. A **45**, 913 (1992).